Received 10 January 2022; revised 24 February 2022; accepted 25 March 2022. Date of publication 31 March 2022; date of current version 8 April 2022.
The review of this article was arranged by Editor A. Nathan

Digital Object Identifier 10.1109/JEDS.2022.3163774

Mobility Enhancement and Abnormal Humps in Top-Gate Self-Aligned Double-Layer Amorphous InGaZnO TFTs

MING-XUAN LEE [1], JIH-CHAO CHIU [1] (Graduate Student Member, IEEE), SONG-LING LI [2], EKNATH SARKAR [1], YU-CIAO CHEN [2], CHIA-CHUN YEN [3], TSANG-LONG CHEN [3], CHENG-HSU CHOU [4], AND C. W. LIU [1,2,5,6] (Fellow, IEEE)

1 Graduate Institute of Electronics Engineering, National Taiwan University, Taipei 106, Taiwan
2 Graduate Institute of Photonics and Optoelectronics, National Taiwan University, Taipei 106, Taiwan
3 Technology Integration Department I, Innolux Corporation, Tainan 744, Taiwan
4 Technology Development Division Group II, Innolux Corporation, Tainan 744, Taiwan
5 Department of Electrical Engineering, National Taiwan University, Taipei 106, Taiwan
6 Graduate School of Advanced Technology, National Taiwan University, Taipei 106, Taiwan

CORRESPONDING AUTHOR: C. W. LIU (e-mail: cliu@ntu.edu.tw; chee@cc.ee.ntu.edu.tw)

This work was supported in part by the Ministry of Science and Technology, Taiwan, under Grant MOST 110-2218-E-A49-013-MBK, Grant MOST 110-2622-8-002-014, and Grant MOST 110-2218-E-002-030; and in part by the Ministry of Education, Taiwan, under Grant NTU-CC-110L892601.

ABSTRACT The mobility enhancement and the positive bias stress of top-gate self-aligned TFTs using the a-IGZO channel with a front barrier are investigated. The a-IGZO front barrier can keep electrons in the a-IGZO channel away from the top-gate oxide to significantly enhance the electron mobility at the top gate operation. The parasitic channel induces a hump in the transfer characteristics. The positive bias stress shifts the hump to the negative voltage abnormally. The H_2O in the polymer film on array layer is responsible for the abnormal shift. The H_2O diffuses into the top-gate insulator and is electrolyzed to create H^+, which forms a parasitic channel with a negative shift of threshold voltage, leading to the abnormal hump. The abnormal humps are increasingly significant with the increasing channel width and the decreasing channel length. The channel width dependence on positive bias stress is due to the inverse narrow width effect caused by the fringe electric field. The channel length dependence on positive bias stress is due to the H^+ diffusion toward the center of the parasitic channel from both the source and drain sides.

INDEX TERMS Positive bias stress (PBS), a-IGZO, hump, polymer film on array (PFA).

I. INTRODUCTION

Thin film transistors (TFTs) are used for the state-of-the-art displays [1]. With the increasing demand on the frame rate and the resolution of displays, TFTs with high mobility are required [2]. Nevertheless, the traditional hydrogenated amorphous silicon (a-Si:H) TFTs show low mobility (< 1 cm^2/V-s) [3] and poor stability [4], making it difficult for advanced applications. In recent years, amorphous indium gallium zinc oxide (a-IGZO) has attracted much attention to be the promising channel material of TFTs for next-generation displays due to the high mobility (> 10 cm^2/V-s), high on/off current ratio, good uniformity in large area, low process temperature (< 400 °C), and low manufacturing cost [5]–[8]. Up to now, the a-IGZO TFTs with several structures have been fabricated, such as a bottom gate structure with etch-stop layer [9], [10], a bottom gate structure with back-channel-etch (BCE) type [11], and a top-gate self-aligned (TG-SA) coplanar structure [12], [13]. The bottom gate structures have the merit of the simple fabrication process. However, the overlap between gate and source/drain (S/D) electrodes causes parasitic capacitance, which reduces the operation speed of the TFT circuits. Therefore, a-IGZO

TFTs with TG-SA coplanar structure are developed to minimize the parasitic capacitance. With the advantages of small parasitic capacitance and channel length scalability, a-IGZO TFTs with TG-SA coplanar structure can meet the requirements of high-pixel density, high-speed response, and large panel size [13]–[15].

In addition to mobility enhancement, the reliability of TFTs is also important for the mass production. a-IGZO itself is sensitive to light, bias stress, and environment [16]–[18]. Humps have serious influence on pixel brightness during the operation [19]. The hump occurs due to the existence of parasitic channels. Abnormal humps have been reported in metal-oxide-semiconductor field-effect transistors (MOSFETs), silicon-on-glass (SiOG) TFTs and low temperature polysilicon (LTPS) TFTs [20]–[22]. Normally, the positive bias stress (PBS) leads to the positive threshold voltage (V_t) shift by trapping electron into gate insulator. The abnormal hump is the occurrence of the negative V_t shift under PBS.

In this work, we take advantage of the band discontinuity of the double-layer a-IGZO to enhance the mobility by the front barrier. The band alignment ensures the carrier confinement. The comparison between the TFTs with and without polymer film on array (PFA) shows that the PFA is responsible for the abnormal hump. The PFA is used as the planarization for pixel electrodes and reduces the parasitic capacitance between gate bus lines and pixel electrodes [23]. The dependence of channel width and channel length on humps is also investigated. Note that the double-layer a-IGZO channel in a BCE TFT with a front barrier was demonstrated to enhance mobility and reliability reportedly [7].

II. EXPERIMENTS

The schematic diagram of the top-gate self-aligned coplanar a-IGZO TFT (not scaled) is shown in Fig. 1. The sputtered 100-nm-thick Al/Mo layer was patterned as the bottom gate electrode, and the 320-nm-thick bottom gate insulator (GI, SiN_X/SiO_X) was deposited by plasma-enhanced chemical vapor deposition (PECVD). The 40 nm a-IGZO channel and the 20 nm a-IGZO front barrier were deposited by a radio frequency magnetron sputter with the Ar/O_2 flows of 50 sccm/6 sccm and 50 sccm/14 sccm, respectively. After patterning the channel, the post deposition annealing (PDA) was performed at 400 °C in air for one hour. The 120-nm-thick SiO_X was deposited as the top GI by PECVD at 260 °C, followed by the 280-nm-thick Ti/Al/Mo layer sputtered on the top GI as the top gate electrode. The top gate and the bottom gate insulators should be thick enough to reduce the parasitic capacitance between the gate bus lines and the data bus lines [24]. After the top GI and metal were patterned, the 300-nm-thick SiO_X layer was deposited as an interlayer dielectric (ILD) by PECVD at 260 °C with high silane flow rate to increase the hydrogen content in ILD, which induces hydrogen diffusion from ILD into a-IGZO S/D regions to form conductive S/D [25]. Afterwards,

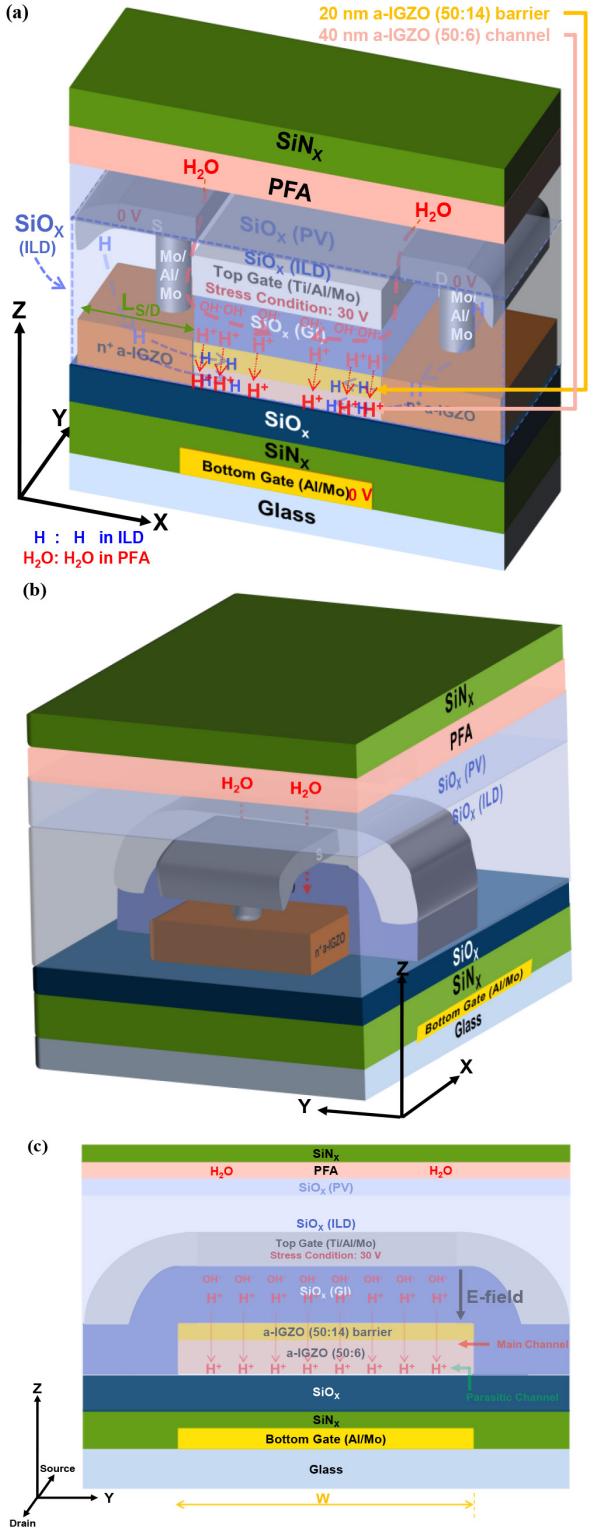

FIGURE 1. (a) Schematic diagram (not scaled) of self-aligned top-gate coplanar a-IGZO TFTs. PFA (polymer film on array) and SiN_X passivation layers protect from moisture permeation. ILD is SiO_X. (b) After 90 degrees rotation about Z axis from (a). (c) Cross-sectional view along the channel width.

the S/D contact holes were formed, and the 370-nm-thick Mo/Al/Mo was sputtered as the S/D metal. The additional 200-nm-thick SiO_X was deposited as the passivation (PV)

layer by PECVD. An organic photo resist polymer film on array (PFA) is used as the planarization for pixel electrodes and reduces the parasitic capacitance between gate bus lines and pixel electrodes [23]. The SiN_X layer was deposited finally to protect the a-IGZO TFT from exterior atmosphere.

III. RESULTS AND DISCUSSION

The role of hydrogen not only acts as a defect passivator to reduce electron traps, but also acts as a shallow donor in a-IGZO [26], [27]. Hydrogen diffusing into the a-IGZO channel first passivates the defect, then excess hydrogen as donors can increase electron density [28]. When the sufficient hydrogen in a-IGZO acts as shallow donors, it can raise the Fermi level (E_F) of a-IGZO [29], [30]. There are more carriers in a-IGZO:H, lowering the effective barrier height in the conduction path [29], [31]. Thus, hydrogen can make the conductive n^+ a-IGZO as the S/D contact regions (Fig. 1(a) and (b), Fig. 1(c) is the cross-sectional view of Fig. 1(b)).

To investigate the effectiveness of the front barrier, the band alignment was measured as shown in Fig. 2. 100-nm a-IGZO films were deposited on glass substrates for the measurements of optical bandgaps, X-ray photoelectron spectroscopy (XPS), and Kelvin probe force microscopy (KPFM). The optical bandgaps are measured by UV-visible (UV-Vis) using Tauc method (Fig. 2(a)). The valence band offsets (E_F-E_V) are obtained by XPS to extrapolate the binding energy of the O 2p features (Fig. 2(b)). The work functions are measured by KPFM (Fig. 2(c)) [7]. Note that the work function of a-IGZO (50:6) and a-IGZO (50:14) is different but very close (~0.002 eV). The carrier concentration measured by Van der Pauw method is higher in a-IGZO (50:6) than in a-IGZO (50:14) (Fig. 2(d)). The band alignment shows that the conduction band discontinuity (ΔEc) is over 3kT (Fig. 2(e)), indicating that the electrons are mostly confined in the a-IGZO, deposited with the Ar/O_2 flow of 50 sccm/6 sccm, where the main channel is located [7]. The Ar/O_2 flow of 50 sccm/14 sccm was used for the deposition of the front a-IGZO barrier. The Weibull plot shows that the field effect mobility (μ_{FE}) at $V_{OV} = 2$ V (Fig. 3(a)) and $V_{OV} = 0.5$ V (Fig. 3(b)) are significantly higher at the top gate operation than the bottom gate operation. The values of μ_{FE} at the Weibull zero point represent the 63% devices with the mobility lower than the specific value. The μ_{FE} was extracted by the following equation:

$$\mu_{FE} = \frac{L(\partial I_D/\partial V_{OV})}{WC_{OX}V_{DS}} \quad (1)$$

where C_{OX} is the oxide capacitance and the V_{OV} is the overdrive voltage ($V_{OV} = V_{GS} - V_t$). L and W represent channel length and channel width, respectively. In percolation conduction, the mobility increases with increasing carrier concentration [34], leading to mobility at $V_{OV} = 2$ V (Fig. 3(a)) higher than 0.5 V (Fig. 3(b)). The conduction band offsets between the BG GI/channel and barrier/TG GI are 2.9

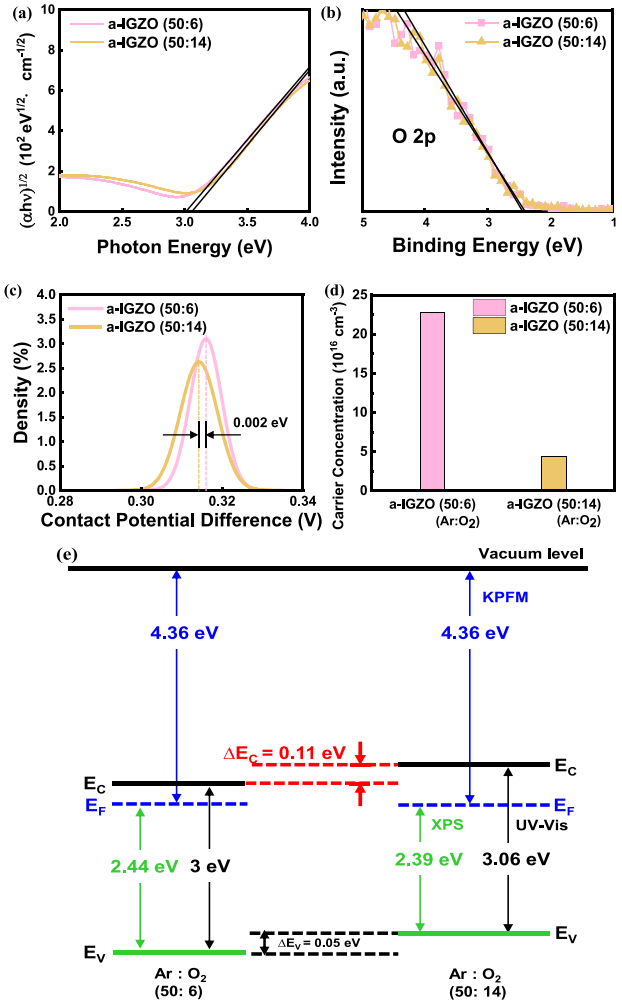

FIGURE 2. (a) Illustration of $(\alpha h\nu)^{1/2}$ versus photon energy to obtain the optical bandgaps of a-IGZO by Tauc method. (b) XPS valence band spectra of a-IGZO. (c) Distribution of CPD in the scan region. (d) Carrier concentration of a-IGZO by Van der Pauw method. (e) The band alignment of the a-IGZO double layers. Ar and O_2 flow rates shown in the parentheses are in order.

and 2.79 eV, respectively, in our simulation. For circuit operation, the voltage-based design is sometimes preferred. The electron densities (Fig. 3(c)) are obtained by simulation at $V_{OV} = 2$ V and 0.5 V for the top gate and bottom gate operation. Note that the thicknesses of the top gate insulator and the bottom gate insulator are different. The mobility at the top $V_{OV} = 0.5$ V is higher than the mobilities at the bottom $V_{OV} = 0.5$ V and 2 V (Fig. 3(a) and (b)), while the density at the top is 3E10 cm^{-2} (Fig. 3(c)) between the densities at the bottom $V_{OV} = 0.5$ V and 2 V. The a-IGZO with the Ar/O_2 flow of 50 sccm/14 sccm was deposited as the front barrier to keep electrons away from the gate oxide/a-IGZO interface to enhance the mobility for the top gate operation (Fig. 3(d)) by reducing the Coulomb scattering, similar to the back-channel-etch TFT [7]. The bottom gate operation (Fig. 3(e)) has no barrier, and thus has low effective mobility. The coulomb scattering is mainly due to the D_{it} at a-IGZO/oxide

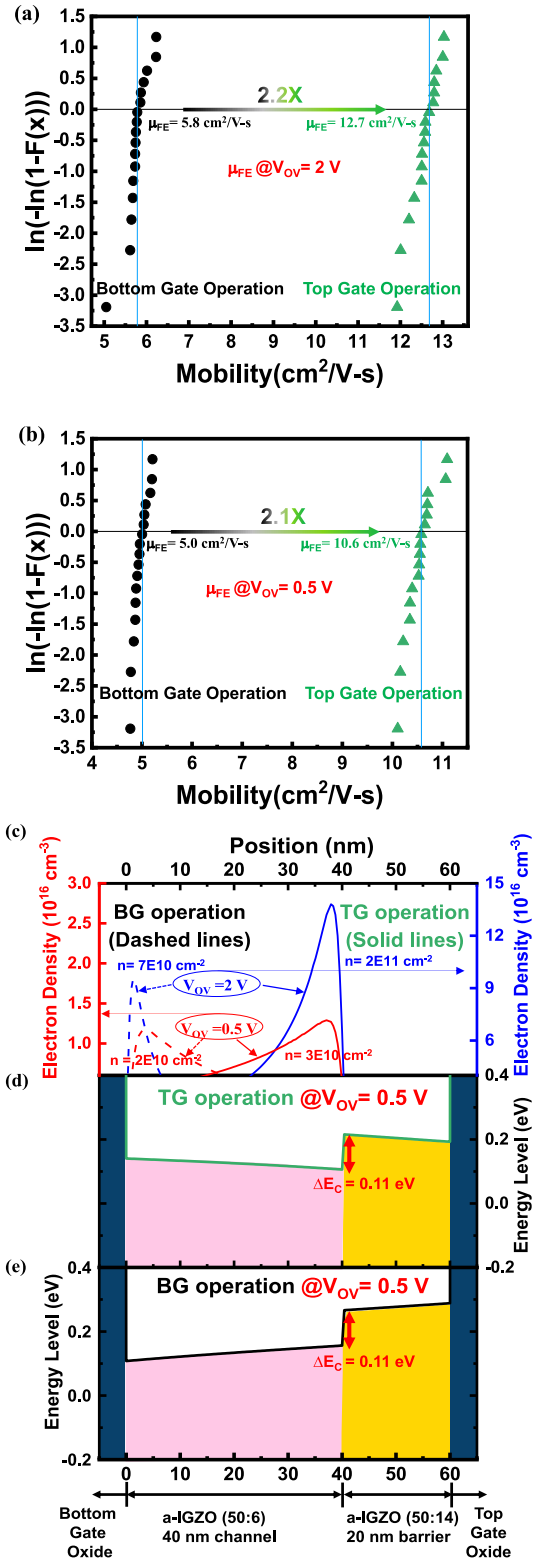

FIGURE 3. **(a) Weibull plot of mobility at V_{OV} = 2 V and (b) V_{OV} = 0.5 V by bottom gate operation and by top gate operation. (c) Electron density distributions and (d) band diagrams of top gate operation and (e) bottom gate operation by TCAD simulation.**

interface and the charge in the boarder of the gate insulator. Therefore, oxide thickness is the second order effect on mobility.

TABLE 1. **Extracted device parameters of TFTs with and without PFA.**

	w/o PFA	w/ PFA
Subthreshold Swing (S.S.) (V/dec)	0.18	0.21

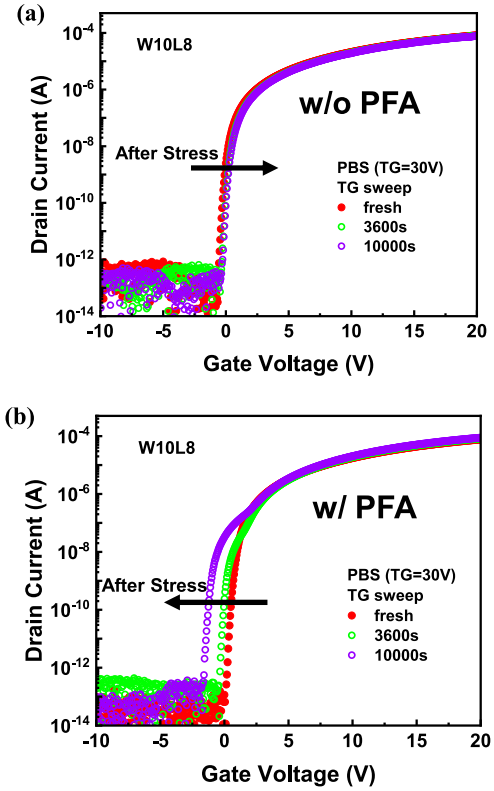

FIGURE 4. **Evolutions of transfer characteristics of the a-IGZO TFTs under PBS of V_{TGS} = 30 V, (a) no PFA layers and (b) with PFA layers. The width is 10 μm, and the length is 8 μm.**

There is no hump in the transfer characteristics of the TFT without PFA under the PBS (V_{TGS} = 30 V with the drain, source, and bottom gate grounded), while there are humps for the one with the PFA layer (Fig. 4). The PFA layer can be a barrier to prevent the H atoms from the SiNx to the a-IGZO channel. Thus, the device without PFA leads to a less defect density due to hydrogen passivation and has a better S.S. (Table 1). Due to the large bandgap (~3eV) of IGZO, the off-state currents are too low to be measured (Fig. 4(a) and (b)). The PFA is used as the planarization for pixel electrodes and reduces the parasitic capacitance between gate bus lines and pixel electrodes [23]. The hump indicates that the V_t of the parasitic channel is more negative than that of the main channel. The PFA layer contains water molecules [23], and the SiO_X passivation layer cannot resist the moisture sufficiently [35]. The H_2O diffusing from the PFA through the ILD into the SiO_X (GI) via the gap between the S/D metal and the gate metal (red dashed arrow in Fig. 1(a)) can be electrolyzed by the electric field to create H^+ to affect the reliability [36]. The larger top gate bias leads to the more negative V_t shift since more H^+ ions are created

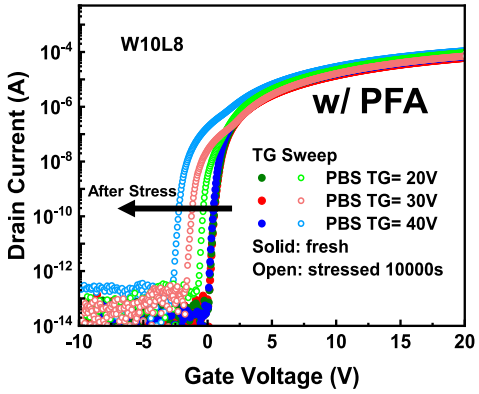

FIGURE 5. **Evolutions of transfer characteristics of the a-IGZO TFTs applying PBS of different V_{TGS} = 20 V, 30 V, and 40 V.**

by the larger electric field (Fig. 5). Since the on-state current is composed of the main channel and the parasitic channel currents, the more negative V_t shift of the parasitic channel results in its higher current due to higher V_{OV}, and the add-on of parasitic channel current into the main channel leads to the increase of on-state current (Fig. 5 and 7(a)). The electric field strength required to electrolyze the H_2O is difficult to be quantitatively measured, but our simulation shows the E-field in our device is 1.6E6 to 3.3E6 V/cm.

Fig. 6(a) shows the width dependence on PBS with the fixed L of 8 μm, which is different from the previously reported result that the abnormal hump has no width dependence [37], [38]. In our work, the negative V_t shift is more serious with increasing channel width. The proposed mechanism of the hump is plotted in Fig. 6(b), a cross section of Fig. 1(b). With applying positive bias on the top gate, more H^+ ions electrolyzed from H_2O in the GI. The created H^+ ions move toward the a-IGZO channel and can penetrate the a-IGZO barrier [39], and the OH^- ions move toward the gate metal [40]. Since the OH^- ions move toward the top gate metal, the OH^- ions near the gate metal have little effect on V_t shift. Thus, we focus on the H^+ ions which move toward the a-IGZO channel. The H^+ can be trapped in the oxygen vacancy sites in a-IGZO and formed positively charged centers [41], [42]. It is our hypothesis that the H^+ ions drift toward the channel and then segregate at the bottom a-IGZO via oxygen vacancies to form a parasitic channel since the underneath SiO_X has much fewer oxygen vacancies than a-IGZO [43] and has no preference to trap H^+ ions. The channel width dependence can be explained by the inverse narrow width effect [44]. The extra fringe electric field (Fig. 6(b)) makes the effective area C_{OX} smaller in the device with larger channel width (Fig. 6(c)), leading to the more negative V_t shift. Therefore, the negative V_t shift increases with increasing channel width. Note that

$$\Delta V_t = -\frac{qN_D t_{ch}}{C_{OX}} \tag{2}$$

where N_D is the total ionized charge density including H^+, t_{ch} is the channel thickness, and C_{OX} is the areal capacitance.

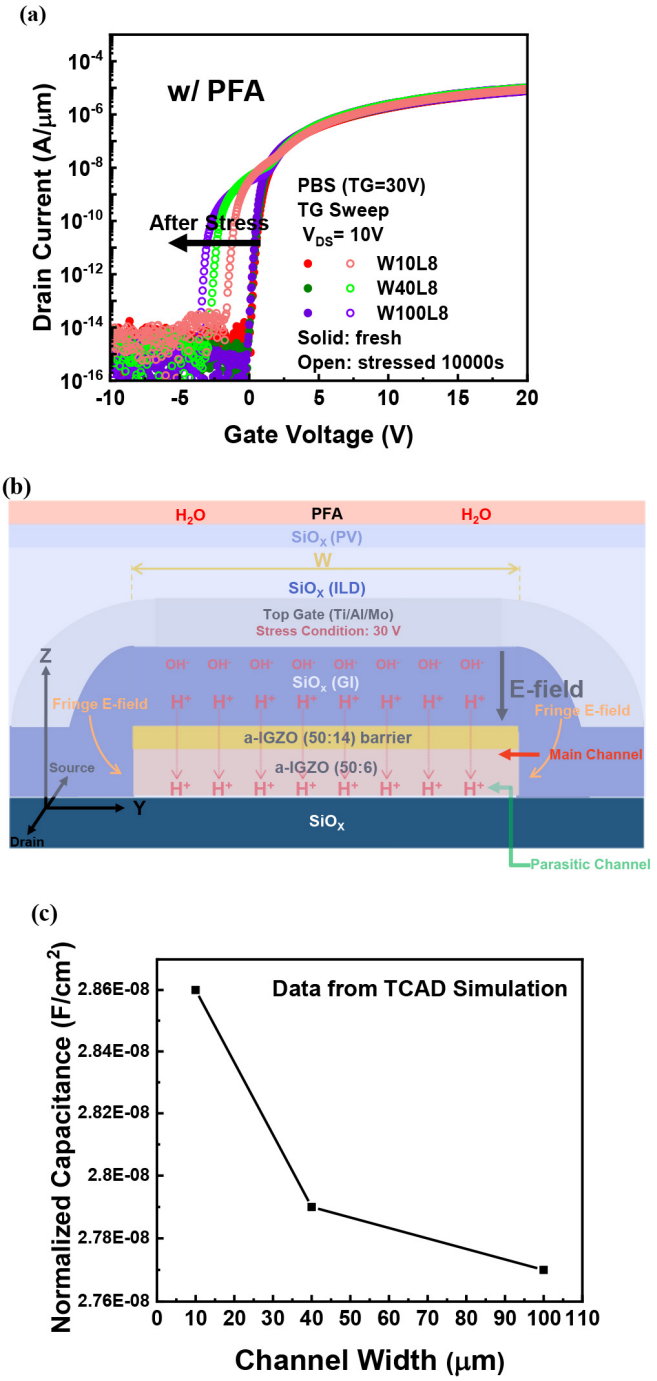

FIGURE 6. **(a) Transfer characteristics of the fresh and stressed a-IGZO TFTs with fixed channel length of 8 μm and different channel widths. (b) Proposed mechanism and H^+ along the channel width. (c) Areal capacitance extracted by TCAD simulation.**

After PBS, the ΔV_t between the channel widths of 10 μm and 100 μm is around 1.9 V, and the ΔV_t between the channel widths of 40μm and 100 μm is around 0.7 V. Based on the simulated C_{OX} (Fig. 6), the N_D is estimated to be ~6E18 cm^{-3} assuming the t_{ch} of the parasitic channels is 20 nm.

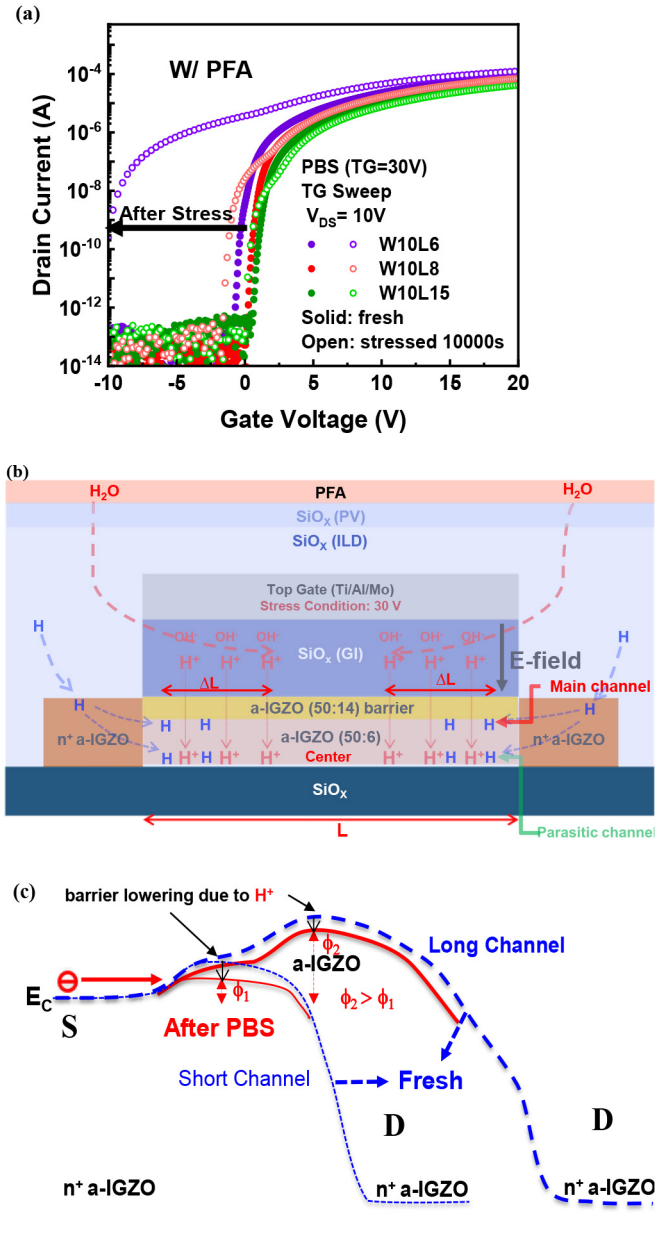

FIGURE 7. Evolutions of normalized (I_D x L/W) transfer characteristics of the a-IGZO TFTs with channel length of (a) 6 μm, 8 μm, and 15 μm under the PBS of V_{TGS} = 30 V. (b) Proposed mechanism and H^+ and H along the channel length. (c) Band diagrams for short channel vs long channel. Blue dashed lines are fresh condition for main channels (no humps) due to H diffusion, and red solid lines are after PBS for parasitic channels due to H^+ diffusion. Note that the parasitic channel has small barrier lowering in the long channel than the short channel.

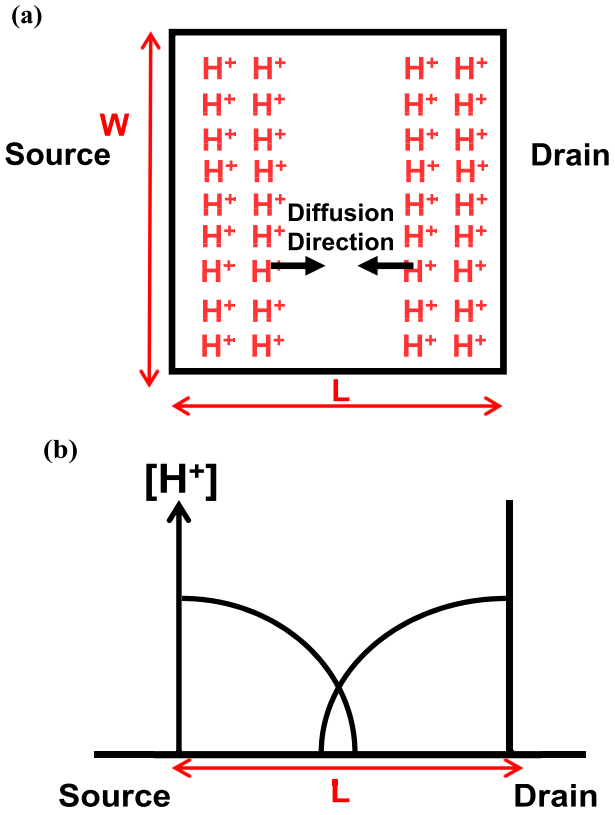

FIGURE 8. (a) Schematics of H^+ diffusion to form parasitic channel during PBS. (b) Schematics of H^+ diffusion profile in the parasitic channels.

The fresh V_t of the main channel before PBS is more negative for the shorter channel (solid symbol lines in Fig. 7(a)) due to additional hydrogen atoms diffusion during the formation of the conductive S/D [45], as indicated by blue H in Fig. 7(b). The H diffusion from S/D reduces the barrier more significantly for the shorter channel (dashed lines in Fig. 7(c)). After PBS, the H^+ is created and almost has no effect on the main channel because the electric field makes the H^+ move toward the bottom parasitic channel. Some H^+ ions are trapped in the oxygen vacancy sites at the bottom a-IGZO channel, while some are not be trapped. These untrapped H^+ ions diffuse laterally to the center of parasitic channels due to the concentration gradient from both the source and drain sides (Fig. 8(a) and (b)). The parasitic channel of the TFT with the shorter channel has the larger V_t shift (open symbol lines in Fig. 7(a)). The H^+ can reach closer to the center of the parasitic channel in the shorter channel device from both the source and drain sides (Fig. 7(b)). In consequence, the effective barrier height lowering is more serious at the center with the shorter channel after PBS (red solid lines in Fig. 7(c)). Fig. 7 (c) is the common conceptual diagram to explain short channel effects [46], and this hydrogen effect on negative V_t shift due to the barrier height lowering recently reported in the IGZO TFT [29]. Therefore, the negative V_t shift increases significantly with decreasing channel length. Note that the V_t of the main channel with L = 15 μm (Fig. 7(a)) has the slightly positive shift after PBS due to the small H^+ effect in the long channel device, leading to the normally positive V_t shift by trapping electron into the gate oxide.

Based on our width (Fig. 6) and length (Fig. 7) dependence on V_t shift of the parasitic channels, it seems that the diffusion length of H^+ for the stress time of 10000 s is around 15μm/2 ≈ 7.5μm because the hump of the TFT with L = 15 μm and W = 10 μm is very mild (Fig. 7(a)),

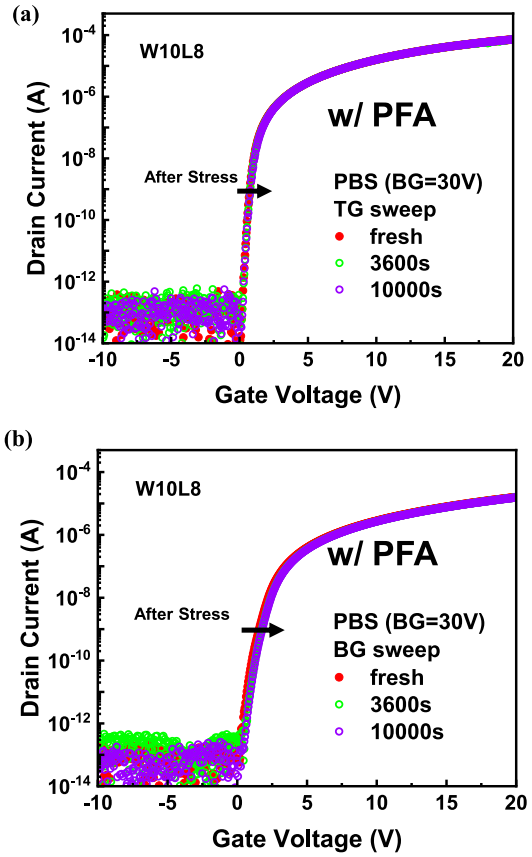

FIGURE 9. **Evolutions of transfer characteristics of the a-IGZO TFT under PBS of V_{BGS} = 30 V with PFA layers (a) by top gate operation and (b) by bottom gate operation. The width is 10 μm, and the length is 8 μm.**

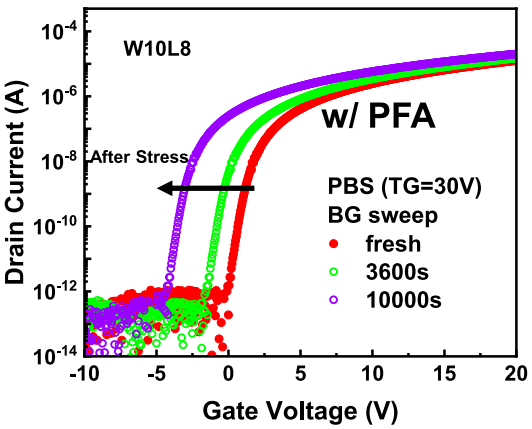

FIGURE 10. **Evolutions of transfer characteristics of the a-IGZO TFT under PBS of V_{TGS} = 30 V by bottom gate operation with PFA layers. The width is 10 μm, and the length is 8 μm.**

i.e., at the edge of parasitic channel formation. All devices in Fig. 6(b) have the L = 8 μm, the H^+ diffusion profile (Fig. 8) merges from both the source and drain sides to form a complete parasitic channel.

Since the ILD SiO_X is far away from the bottom gate insulator (Fig. 1(a), $L_{S/D}$ = 10 μm), the H_2O cannot reach the bottom gate insulator. There is no negative V_t shift after PBS stress (V_{BGS} = 30 V with the drain, source, and bottom gate grounded) (Fig. 9). The positive shift is smaller by top gate operation (Fig. 9(a)) than bottom gate operation (Fig. 9(b)) since the front barrier can reduce electron traps into the top SiO_X.

There are negative V_t shifts without humps after PBS of V_{TGS} = 30 V by bottom gate operation (Fig. 10). This indicates that the created H ions in the top gate insulator move to the bottom channel, where electrons and H ions are close to each other to form one channel, no parasitic. For the gate operation, there are electrons near the top channel to form the main channel, while some electrons are attracted by H ions at the bottom channel to form the parasitic channel. This supports our hypothesis of the H ion penetration.

IV. CONCLUSION

The mobility can be enhanced (2.1X) with a front barrier. The abnormal hump is attributed to the H_2O in the organic PFA layer. Under applying PBS, the H^+ ions are created to form the parasitic channels, resulting in the abnormal humps. The negative V_t shift of the humps increases with increasing channel width and decreasing channel length.

REFERENCES

[1] S. Samanta *et al.*, "Amorphous InGaZnO thin-film transistors with sub-10-nm channel thickness and ultrascaled channel length," *IEEE Trans. Electron Devices*, vol. 68, no. 3, pp. 1050–1056, Mar. 2021, doi: 10.1109/TED.2020.3048920.

[2] T. Kamiya, K. Nomura, and H. Hosono, "Present status of amorphous In-Ga-Zn-O thin-film transistors," *Sci. Technol. Adv. Mater.*, vol. 11, no. 4, pp. 1–23, Sep. 2010, doi: 10.1088/1468-6996/11/4/044305.

[3] C. Lo, Z.-L. Feng, W.-L. Huang, C. W. Liu, T.-L. Chen, and C.-H. Chou, "Abnormal threshold voltage shift of amorphous InGaZnO thin-film transistors due to mobile sodium," *IEEE J. Electron Devices Soc.*, vol. 4, no. 5, pp. 353–357, Sep. 2016, doi: 10.1109/JEDS.2016.2562675.

[4] S. M. Jahinuzzaman, A. Sultana, K. Sakariya, P. Servati, and A. Nathan, "Threshold voltage instability of amorphous silicon thin-film transistors under constant current stress," *Appl. Phys. Lett.*, vol. 87, no. 2, Jul. 2005, Art. no. 23502, doi: 10.1063/1.1993766.

[5] C.-C. Yen, A.-H. Tai, Y.-C. Liu, T.-L. Chen, C.-H. Chou, and C. W. Liu, "Oxygen-related reliability of amorphous InGaZnO thin film transistors," *IEEE J. Electron Devices Soc.*, vol. 8, pp. 540–544, 2020, doi: 10.1109/JEDS.2020.2993018.

[6] T. Kamiya and H. Hosono, "Material characteristics and applications of transparent amorphous oxide semiconductors," *NPG Asia Mater.*, vol. 2, no. 1, pp. 15–22, Jan. 2010, doi: 10.1038/asiamat.2010.5.

[7] A.-H. Tai, C.-C. Yen, T.-L. Chen, C.-H. Chou, and C. W. Liu, "Mobility enhancement of back-channel-etch amorphous InGaZnO TFT by double layers with quantum well structures," *IEEE Trans. Electron Devices*, vol. 66, no. 10, pp. 4188–4192, Oct. 2019, doi: 10.1109/TED.2019.2932798.

[8] T.-L. Chen, K.-C. Huang, H.-Y Lin, C.-H. Chou, H. H. Lin, and C. W. Liu, "Enhanced current drive of double-gate α-IGZO thin-film transistors," *IEEE Electron Device Lett.*, vol. 34, no. 3, pp. 417–419, Mar. 2013, doi: 10.1109/LED.2013.2238884.

[9] M. Nag *et al.*, "High performance a-IGZO thin-film transistors with mf-PVD SiO_2 as an etch-stop-layer," *J. Soc. Inf. Display*, vol. 22, no. 1, pp. 23–28, Apr. 2014, doi: 10.1002/jsid.212.

[10] L. Lu and M. Wong, "A bottom-gate indium-gallium-zinc oxide thin-Film transistor with an inherent etch-stop and annealing-induced source and drain regions," *IEEE Trans. Electron Devices*, vol. 62, no. 2, pp. 574–579, Feb. 2015, doi: 10.1109/TED.2014.2375194.

[11] M. Nag *et al.*, "Back-channel-etch amorphous indium–gallium–zinc oxide thin-film transistors: The impact of source/drain metal etch and final passivation," *Jpn. J. Appl. Phys.*, vol. 53, no. 11, pp. 1–5, Nov. 2014, doi: 10.7567/JJAP.53.111401.

[12] C.-H. Wu, H.-H. Hsieh, C.-W. Chien, and C.-C. Wu, "Self-aligned top-gate coplanar In-Ga-Zn-O thin-film transistors," *J. Display Technol.*, vol. 5, no. 12, pp. 515–519, Dec. 2009, doi: 10.1109/JDT.2009.2026189.
[13] Y. Takeda *et al.*, "Development of high mobility top gate IGZO-TFT for OLED display," *SID Symp. Dig. Tech. Papers*, vol. 50, no. 1, pp. 516–519, May 2019, doi: 10.1002/sdtp.12970.
[14] Y.-C. Wu *et al.*, "Design of an advanced bottom-emission AMOLED display for TVs with high-PPI and large size," *SID Symp. Dig. Tech. Papers*, vol. 50, no. 1, pp. 941–944, Jun. 2019, doi: 10.1002/sdtp.13080.
[15] J. Jeong, Y. Hong, J. K. Jeong, J.-S. Park, and Y.-G. Mo, "MOSFET-like behavior of a-InGaZnO thin-film transistors with plasma-exposed source–Drain Bulk region," *J. Display Technol.*, vol. 5, no. 12, pp. 495–500, Dec. 2009, doi: 10.1109/JDT.2009.2021490.
[16] M. D. H. Chowdhury, P. Migliorato, and J. Jang, "Light induced instabilities in amorphous Indium–Gallium–Zinc–Oxide thin-film transistors," *Appl. Phys. Lett.*, vol. 97, no. 17, pp. 1–3, Oct. 2010, doi: 10.1063/1.3503971.
[17] A. Suresh and J. F. Muth, "Bias stress stability of indium gallium zinc oxide channel based transparent thin film transistors," *Appl. Phys. Lett.*, vol. 92, no. 3, pp. 1–3, Jan. 2008, doi: 10.1063/1.2824758.
[18] J.-S. Park, J. K. Jeong, H.-J. Chung, Y.-G. Mo, and H. D. Kim, "Electronic transport properties of amorphous indium-gallium-zinc oxide semiconductor upon exposure to water," *Appl. Phys. Lett.*, vol. 92, no. 7, pp. 1–3, Feb. 2008, doi: 10.1063/1.2838380.
[19] Y.-M. Kim *et al.*, "Investigation of zinc interstitial ions as the origin of anomalous stress-induced hump in amorphous indium gallium zinc oxide thin film transistors," *Appl. Phys. Lett.*, vol. 102, no. 17, Apr. 2013, Art. no. 173502, doi: 10.1063/1.4803536.
[20] M. Carmona *et al.*, "MOSFET layout modifications for hump effect removal," *Microelectron. Eng.*, vol. 109, pp. 168–171, Sep. 2013, doi: 10.1016/j.mee.2013.03.109.
[21] M. Mativenga *et al.*, "Degradation model of self-heating effects in silicon-on-glass TFTs," *IEEE Trans. Electron Devices*, vol. 58, no. 8, pp. 2440–2447, Aug. 2011, doi: 10.1109/TED.2011.2155068.
[22] A. Valletta, P. Gaucci, L. Mariucci, G. Fortunato, and F. Templier, "'Hump' characteristics and edge effects in polysilicon thin film transistors," *J. Appl. Phys.*, vol. 104, no. 12, Dec. 2008, Art. no. 124511, doi: 10.1063/1.3050323.
[23] S.-M. Ge *et al.*, "Development of CU BCE-Structure IGZO TFT for a high-ppi 31-in. 8K x 4K GOA LCD," *SID Symp. Dig. Tech. Papers*, vol. 48, pp. 592–595, May 2017, doi: 10.1002/sdtp.11705.
[24] W.-S. Hong, K.-W. Jung, J.-H. Choi, B.-K. Hwang, and K. Chung, "High transmittance TFT-LCD panels using high transmittance TFT-LCD panels using low-/spl kappa/ CVD films CVD films," *IEEE Electron Device Lett.*, vol. 25, no. 6, pp. 381–383, Jun. 2004, doi: 10.1109/LED.2004.828957.
[25] A. Sato *et al.*, "Amorphous In-Ga-Zn-O thin-film transistor with coplanar homojunction structure," *Thin Solid Films*, vol. 518, no. 4, pp. 1309–1313, Dec. 2009, doi: 10.1016/j.tsf.2009.01.165.
[26] Y. Hanyu *et al.*, "Hydrogen passivation of electron trap in amorphous In-Ga-Zn-O thin-film transistors," *Appl. Phys. Lett.*, vol. 103, no. 20, Nov. 2013, Art. no. 202114, doi: 10.1063/1.4832076.
[27] H.-Y. Noh, J. Kim, J.-S. Kim, M.-J. Lee, and H.-J. Lee, "Role of hydrogen in active layer of oxide-semiconductor-based thin film transistors," *Crystals*, vol. 9, no. 2, p. 75, Jan. 2019, doi: 10.3390/cryst9020075.
[28] T. T. T. Nguyen, B. Aventurier, O. Renault, T. Terlier, J. P. Barnes, and F. Templier, "Impact of hydrogen diffusion on electrical characteristics of IGZO TFTs passivated by SiO2 or Al2O3," in *Proc. 21st Int. Workshop Active-Matrix Flatpanel Displays Devices (AM-FPD)*, 2014, pp. 149–152, doi: 10.1109/AM-FPD.2014.6867154.
[29] H.-C. Chen *et al.*, "Hydrogen diffusion and threshold voltage shifts in top-gate amorphous InGaZnO thin-film transistors," *IEEE Trans. Electron Devices*, vol. 67, no. 8, pp. 3123–3128, Aug. 2020, doi: 10.1109/TED.2020.2998101.
[30] G.-F. Chen *et al.*, "Abnormal dual channel formation induced by hydrogen diffusion from SiNx interlayer dielectric in top gate a-InGaZnO transistors," *IEEE Electron Device Lett.*, vol. 38, no. 3, pp. 334–337, Mar. 2017, doi: 10.1109/LED.2017.2657546.
[31] H.-C. Chen *et al.*, "Abnormal hump effect induced by hydrogen diffusion during self-heating Stress in top-gate amorphous InGaZnO TFTs," *IEEE Trans. Electron Devices*, vol. 67, no. 7, pp. 2807–2811, Jul. 2020, doi: 10.1109/TED.2020.2994539.
[32] M. Mativenga, F. Haque, Billah, M. M. Billah, and J. G. Um, "Origin of light instability in amorphous IGZO thin-film transistors and its suppression," *Sci. Rep.*, vol. 11, Jul. 2021, Art. no. 14618, doi: 10.1038/s41598–021-94078–8.
[33] G. Wakimura, Y. Yamauchi, T. Matsuoka, and Y. Kamakura, "Mechanism of off-leakage current in InGaZnO thin-film transistors," in *Proc. IEEE Int. Meeting Future Electron Devices, Kansai (IMFEDK)*, Jun. 2014, pp. 1–2, doi: 10.1109/IMFEDK.2014.6867062.
[34] K. Nomura, H. Ohta, A. Takagi, T. Kamiya, M. Hirano, and H. Hosono, "Room-temperature fabrication of transparent flexible thin-film transistors using amorphous oxide semiconductors," *Nature*, vol. 432, pp. 488–492, Nov. 2004, doi: 10.1038/nature03090.
[35] M. D. H. Chowdhury *et al.*, "Effect of SiO_2 and SiO_2/SiN_x passivation on the stability of amorphous indium-gallium zinc-oxide thin-film transistors under high humidity," *IEEE Trans. Electron Devices*, vol. 62, no. 3, pp. 869–874, Mar. 2015, doi: 10.1109/TED.2015.2392763.
[36] H.-C. Chen *et al.*, "Investigation of the capacitance−voltage electrical characteristics of thin-film transistors caused by hydrogen diffusion under negative bias stress in a moist environment," *ACS Appl. Mater. Interfaces*, vol. 11, pp. 40196–40203, Nov. 2019, doi: 10.1021/acsami.9b11637.
[37] M. Mativenga, M. Seok, and J. Janga, "Gate bias-stress induced hump-effect in transfer characteristics of amorphous-indium-galium-zinc-oxide thin-fim transistors with various channel widths," *Appl. Phys. Lett.*, vol. 99, no. 12, Sep. 2011, Art. no. 122107, doi: 10.1063/1.3641473.
[38] J. Yang *et al.*, "Investigation of a hump phenomenon in back-channel-etched amorphous In-Ga-Zn-O thin-film transistors under negative bias stress," *IEEE Electron Device Lett.*, vol. 38, no. 5, pp. 592–595, May 2017, doi: 10.1109/LED.2017.2686898.
[39] Y. Lee *et al.*, "Hydrogen barriers based on chemical trapping using chemically modulated Al_2O_3 grown by atomic layer deposition for InGaZnO thin-film transistors," *ACS Appl. Mater. & Interfaces*, vol. 11, pp. 20349–20360, Apr. 2021, doi: 10.1021/acsami.1c02597.
[40] J.-C. Jhu *et al.*, "Investigation of hydration reaction-induced protons transport in etching-stop a-InGaZnO thin-film transistors," *IEEE Electron Device Lett.*, vol. 36, no. 10, pp. 1050–1052, Oct. 2015, doi: 10.1109/LED.2015.2466103.
[41] J.-Y. Lee, F. Shan, H.-S. Kim, and S.-J. Kim, "Effect of femtosecond laser postannealing on a-IGZO thin-film transistors," *IEEE Trans. Electron Devices*, vol. 68, no. 7, pp. 3371–3378, Jul. 2021, doi: 10.1109/TED.2021.3077344.
[42] M. D. H. Chowdhury *et al.*, "Effect of SiO_2 and SiO_2/SiN_X passivaiton on the stability of amorphous indium-gallium zinc-oxide thin-film transistors under high humidity," *IEEE Trans. Electron Devices*, vol. 62, no. 3, pp. 869–874, Mar. 2015, doi: 10.1109/TED.2015.2392763.
[43] M. Chun, J. G. Um, M. S. Park, M. D. H. Chowdhury, and J. Jang, "Effect of top gate potential on bias-stress for dual gate amorphous indium-gallium-zunc-oxide thin film transistor," *AIP Adv.*, vol. 6, no. 7, pp. 075217-1–075217-8, Jul. 2016, doi: 10.1063/1.4960014.
[44] N. Shigyo and T. Hiraoka, "A review of narrow-channel effects for STI MOSFET's: A difference between surface-and buried-channel cases," *Solid-State Electron.*, vol. 43, no. 11, pp. 2061–2066, 1999, doi: 10.1109/EDL.1986.26422.
[45] D. H. Kang, J. U. Han, M. Mativenga, S. H. Ha, and J. Jang, "Threshold voltage dependence on channel length in amorphous-indium-gallium-zinc-oxide thin-film transistors," *Appl. Phys. Lett.*, vol. 102, no. 8, 2013, Art. no. 083508, doi: 10.1063/1.4793996.
[46] Y. Taur and T. Ning, *Fundamentals of Modern VLSI Devices*, 3rd ed. Cambridge, U.K.: Cambridge Univ. Press., 2021, pp. 206–218, doi: 10.1017/9781108847087.